

AFM study of crystallization and melting of a poly(ethylene oxide) diblock copolymer containing a tablet-like block of poly{2,5-bis[(4-methoxyphenyl)oxycarbonyl]styrene} in ultrathin films

Yun Huang^a, Xuan-Bo Liu^a, Hai-Liang Zhang^{a,1}, Dun-Shen Zhu^a, Yin-Jie Sun^b, Shou-Ke Yan^b, Jing Wang^a, Xiao-Fang Chen^a, Xin-Hua Wan^a, Er-Qiang Chen^{a,*}, Qi-Feng Zhou^{a,*}

^a Department of Polymer Science and Engineering and The Key Laboratory of Polymer Chemistry and Physics of Ministry of Education, College of Chemistry and Molecular Engineering, Peking University, Beijing 100871, China

^b State Key Laboratory of Polymer Physics and Chemistry, Center for Molecular Science, Institute of Chemistry, Chinese Academy of Science, Beijing 100080, China

Received 27 July 2005; received in revised form 7 December 2005; accepted 7 December 2005

Abstract

Crystallization and melting of a poly(ethylene oxide) (PEO) diblock copolymer containing a tablet-like block of poly{2,5-bis[(4-methoxyphenyl)oxycarbonyl]styrene} (PMPCS) in ultrathin films have been studied using atomic force microscopy (AFM) coupled with a hot stage. The PEO and PMPCS block possess the number-average molecular weights (M_n) of 5300 and 2100 g/mol, respectively. The ultrathin films on the mica and glow-discharged carbon surfaces were obtained by static dilute solution casting at room temperature. Isothermal melt crystallization from ultrathin films always leads to flat-on lamellae. Selective area electron diffraction (SAED) experiments have demonstrated that the PEO blocks crystallize with a monoclinic structure identical to that of homo-PEO and the chain direction is perpendicular to the substrate. At $T_c < 44$ °C, the monolayer crystals are dendrites. At $T_c > 48$ °C, square-shaped crystals are formed with the (100) and (020) planes as the crystal edges. At 44 °C $\leq T_c \leq 48$ °C, an intermediate monolayer morphology is observed. The monolayer thickness increases monotonically with increasing T_c . At the same T_c , the monolayer lamellae with the top and bottom amorphous layers contacting with the atmosphere and the substrate possess a significantly larger overall thickness than the long period of the crystals in bulk. For the spiral terraces induced by screw dislocation, the thickness of each terrace is close to that of the monolayer formed at the same T_c , and their melting is mainly determined by the terrace thickness. © 2005 Elsevier Ltd. All rights reserved.

Keywords: Crystallization; PEO diblock copolymer; Ultrathin film

1. Introduction

Polymer crystallization in confined nano-environments, such as in microphase separation structures of block copolymers [1–11] and ultrathin films [12–26], has become an important topic in polymer physics recently. It has been known for years that polymer crystallization from ultrathin films (thickness < 100 nm) on solid substrate can lead to monolayer lamellae, which are used

in the study of single crystal morphology and crystalline structure via microscopy and electron diffraction. The crystallization rate and crystallinity decrease with the decreasing of the film thickness [14–17,24,25]. When the film thickness is very thin (e.g. < 15 nm), the crystalline polymer may remain in under-cooled state for long lifetime [14]. Finger-like or fractal patterns of the monolayer polymer crystals are often seen on solid substrates, and therefore, a mechanism analogous to diffusion limited aggregation has been proposed for the ultrathin film (quasi-two-dimensional) crystallization [18,19,22,23]. After crystallization, the crystallographic c -axis (chain axis) is often perpendicular to the substrate, resulting in flat-on lamellae [13,15–21]. This preferential chain orientation can be long range ordered. For instance, in a thin film of crystalline–amorphous diblock copolymer poly(ethylene oxide)- b -poly(1,4-butadiene) (PEO- b -PBD), the PEO chain orientational registry remains even

* Corresponding authors.

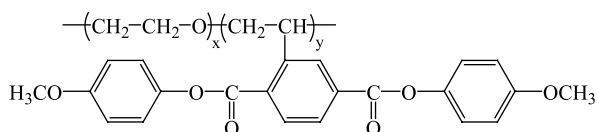
E-mail addresses: eqchen@pku.edu.cn (E.-Q. Chen), qfzhou@pku.edu.cn (Q.-F. Zhou).

¹ Present address: Institute of Polymer Science, Xiangtan University, Xiangtan, Hunan 411105, China.

when the multiple PEO lamellae are separated by the amorphous PBD layer of approximately 10 nm [13].

As a model system for polymer crystallization, the low molecular weight (LMW) PEO with narrow molecular weight distribution has been extensively studied for over 30 years [27,28]. In bulk crystallization, the LMW PEO forms integral folding chain (IF) crystals in the low undercooling (ΔT) region. Recently, the IF crystals of LMW PEO have been also observed in ultrathin films [18,19,21,26]. The lamellar thickness is measured to be identical to an integral fraction of the extended chain length of PEO, revealing that the PEO crystallization from ultrathin films adopt the fashion of chain folding, and moreover, the chain axis is along the surface normal of the substrates. For the LMW PEO diblock copolymers with a microphase-separated lamellar structure, the crystalline chain orientation in ultrathin films may be either perpendicular or parallel to the substrate surface, depending on the PEO crystallization kinetics. From a thermodynamic point of view, a lamellar structure parallel to the substrate is more stable. The crystalline stems therein are ‘standing up’, facilitating the formation of PEO crystals with large lateral dimension. However, it was reported in a LMW hydrogenated polybutadiene-*b*-poly(ethylene oxide) (PB_h-*b*-PEO), the lamellar phase structure originally parallel to the substrate in molten state turned to be vertical after the PEO crystallization at a relatively high growth rate [21]. In this case, the PEO chains were more or less ‘lying down’, resulting in edge-on lamellae.

In this article, we have investigated the crystallization of a diblock copolymer containing a block of LMW PEO and a short block of poly{2,5-bis[(4-methoxyphenyl)oxycarbonyl]-styrene} (PMPCS) from ultrathin films. The chemical structure of the PEO-*b*-PMPCS is shown below.



The number-average MWs (M_n) of the PEO and PMPCS blocks are 5300 and 2100 g/mol, respectively, corresponding to the degree of polymerizations (DP) $x=120$ and $y=5$. In the PMPCS block, each mesogenic side group is laterally attached (jacketed) to the polyethylene backbone via a single carbon-carbon bond [29]. In our previous research on the same PEO-*b*-PMPCS sample [30], we have demonstrated that the short PMPCS block was amorphous and miscible with the PEO block in the melt state. Due to its low DP and the mesogen jacketing effect, the PMPCS block is rather rigid and tablet-like, with a thickness of less than 1.2 nm (corresponding to five repeating units) and a diameter of approximately 1.7 nm (estimated from wide angle X-ray diffraction results). In bulk crystallization, the PMPCS tablets greatly affect the PEO crystallization kinetics and crystal morphology. Particularly, in a wide ΔT range ($14^\circ\text{C} < \Delta T < 30^\circ\text{C}$), the PEO-*b*-PMPCS exhibits square-shaped crystals that are very much different from the typical morphologies of the LMW homo-PEOs. The PMPCS tablets rejected to lamellar fold surfaces prevent the non-integral folding chain (NIF) crystals of PEO blocks from transforming into the IF ones.

Upon using atomic force microscopy (AFM) coupled with a hot stage, this research is concerned with the PEO-*b*-PMPCS monolayer crystals on mica and glow-discharged carbon surfaces. In the ultrathin films of the PEO-*b*-PMPCS, the isothermal crystallization leads to flat-on monolayer crystals that are ‘sandwich’ structured, with the top and bottom amorphous layers contacting with the atmosphere and the substrate, respectively. The morphology and melting behavior of the monolayer crystals are systematically measured as functions of crystallization temperature (T_c). Comparisons of the monolayer thickness (includes two amorphous and one crystalline layers) and the monolayer melting temperatures (T_m) with the long period and T_m of the lamellae from bulk crystallization have been carried out to understand the effect of ‘sandwich’ structure on the monolayer crystals.

2. Experimental section

2.1. Materials and sample preparations

The PEO-*b*-PMPCS block copolymer was synthesized by atom transfer radical polymerization (ATRP) using a PEO-macroinitiator. The synthesis procedure and the chemical structure characterization of the PEO-*b*-PMPCS have been described in Ref. [30]. The M_n s of the precursor PEO and the composition of the PEO-*b*-PMPCS were determined by ^1H NMR (Bruker ARX400 spectrometer, DCCl_3 as solvent and TMS as internal standard). The MW distribution of the sample was measured by gel permeation chromatography (GPC, Waters 150C) calibrated with polystyrene standards. The M_n s of the PEO and PMPCS blocks are 5300 and 2100 g/mol, respectively; the polydispersity of the diblock copolymer is 1.07.

The ultrathin film samples of the PEO-*b*-PMPCS on freshly cleaved mica and carbon-coated mica surfaces were prepared by static solution casting method. Typically, a drop ($\sim 5\ \mu\text{l}$) of the diblock copolymer THF solution at a concentration of 5×10^{-4} g/ml was pipetted onto the substrates at around 25°C ; the excess solution was blotted by filter paper. Each sample was dried under ambient conditions and later in vacuum for days. To improve the surface hydrophilicity and thus the wetting of the PEO-*b*-PMPCS, we performed glow discharge on the carbon surfaces prior to the static solution casting.

2.2. Equipment and experiments

AFM (DI NanoScope IIIa) coupled with a hot stage was utilized to study the morphology and the melting behavior of the PEO-*b*-PMPCS lamellae formed on the solid substrates. The temperature of the AFM hot stage was calibrated using standard materials to have an accuracy of $\pm 0.2^\circ\text{C}$. The height and phase images of the lamellar crystals were recorded using AFM tapping mode, wherein the cantilever force was controlled to be large enough to explore the surface features, yet small enough to avoid the sample damage. The isothermal crystallization was conducted by quenching the samples from the isotropic melt to a preset T_c that is below 30°C . For $T_c > 30^\circ\text{C}$,

a self-seeding technique was applied to promote the crystallization process [31]. The as-cast ultrathin films or the crystals grown at room temperature were heated to a self-seeding temperature (T_s) of 54.5 °C, and then the temperature of the AFM hot stage was rapidly jumped to a desired T_c for isothermal crystallization. To examine the melting behavior, the samples were directly heated on the AFM hot stage after crystallized at different T_c s. When approaching T_m , the AFM images were recorded at every 0.2 °C, with an average heating rate of 0.04 °C/min (the samples were isothermally stayed 5 min at each temperature for AFM scanning).

The chain orientation of the monolayer crystals was examined by selective area electron diffraction (SAED). The experiments were performed using transmission electron microscope (TEM, JEM-100CX) with an accelerating voltage of 100 kV. The samples on the carbon surfaces were further protected with a second layer of carbon before floating off on water. After transferred to copper TEM grids, the samples were dried in vacuum for 24 h at room temperature. A polyethylene (PE) decoration method was employed to study the fold surface structure of the monolayer crystals [32,33], where a linear PE sample with M_n of 12 kg/mol was used. During the decoration, an optimal 10 cm distance between the sample and the basket was chosen in the vacuum evaporator. PE was degraded, evaporated, deposited, and crystallized on the sample surface.

3. Results and discussion

Fig. 1(a) shows an AFM image of an as-cast ultrathin film of the PEO-*b*-PMPCS diblock copolymer on the mica surface. The uniform dendritic monolayer is 11 nm thick (Fig. 1(b)). When the carbon films were used, we found that the surface hydrophilicity is crucial for preparing the ultrathin films via the simple static solution casting method. The direct solution casting on the fully hydrophobic carbon surface made the diblock copolymer dewetted thereon. Consequently, droplets appeared with heights ranging from 20 to 60 nm after complete removal of the solvent, and no crystalline feature was present even after the samples were stored at –20 °C for days. This implied that the high surface tension of the droplets prevented them from crystallization, making the droplets very difficult to

turn into lamellar morphology. In this case, the diblock copolymer was trapped in the metastable state of undercooled melt. To improve the surface hydrophilicity and thus the wetting of the PEO-*b*-PMPCS, the carbon surfaces were treated by glow discharge prior to the solution casting. The as-cast ultrathin films on the glow-discharged carbon surfaces presented the same morphology as that shown in Fig. 1(a); moreover, the monolayer thickness was also 11 nm. On both the mica and glow-discharged carbon surfaces, the as-cast monolayer dendrites look like flat-on lamellae. The SAED experiments of the as-cast samples on glow-discharged carbon surface demonstrated two pairs of strong diffractions corresponding to the {120} planes of the monoclinic crystalline lattice of PEO [34]. This indicates that in the crystals of PEO blocks, the PEO chain direction is parallel to the electron beam, i.e. to the surface normal of the substrate. Since their morphology is highly similar to that on the carbon surface, we consider that the as-cast monolayers on the mica surface also crystallized with the same PEO chain orientation.

In addition to the flat-on lamellar morphology, the as-cast samples of the PEO-*b*-PMPCS on the mica surface may also present needle-like crystals, as shown in Fig. 2(a). However, such morphology has never been observed on the glow-discharged carbon surface that is less hydrophilic than the mica surface. The AFM phase image (Fig. 2(a)) shows that the needle-like crystals are packed parallel to each other, wherein the phase contrast should be mainly attributed to the different viscoelastic properties between the crystalline PEO cores and the amorphous portions. The periodicity between the bright lines is 8–14 nm; the height (vertical dimension) of the needle-like crystals varies from 20 to 50 nm. This morphology is highly reminiscent of the edge-on lamellae grown in thin films, implying the crystalline chain orientation preferentially parallel to the substrate. We suspect that on the mica surface, the relatively strong hydrophilic–hydrophilic interaction helps the PEO segments to lie down when the PEO-*b*-PMPCS molecules are absorbed. During the very fast crystallization induced by the solvent evaporation, some PEO segments may have no enough time to adjust their orientation from ‘lying down’ to ‘standing up’, giving the needle-like or edge-on crystals. However, due to the restriction of the film thickness,

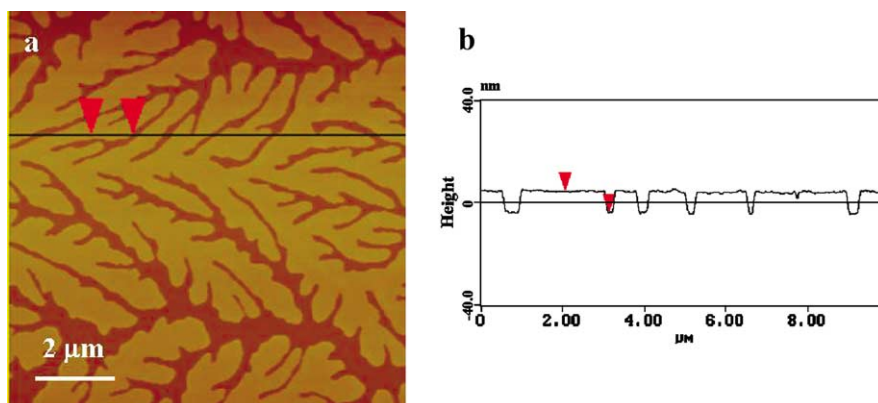


Fig. 1. (a) AFM height image of an as-cast ultrathin film of the PEO-*b*-PMPCS on the mica surface. (b) The height profile along the straight line in (a). The height difference between the two red arrows is 11 nm (for interpretation of the reference to colour in this legend, the reader is referred to the web version of this article).

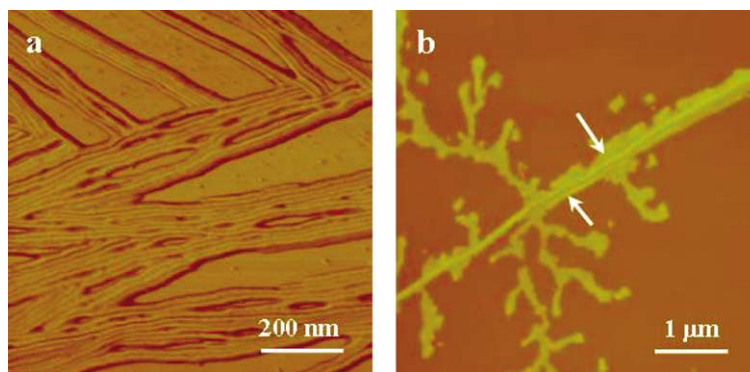


Fig. 2. (a) AFM phase image of needle-like (edge-on) crystals on the mica surface obtained after the solution casting. (b) AFM height image of the sample quenched to room temperature after controlled melting of the needle-like crystals. Two 'needles' (pointed by the arrows) were preserved upon heating.

the growth of the edge-on crystals along the mica surface normal is limited. The very small vertical dimension of 20–50 nm makes the needle-like crystals less stable compared with the flat-on lamellae. No needle-like crystals were found in the ultrathin film via isothermal melt crystallization. Fig. 2(b) describes an AFM result of a sample quenching to room temperature after a controlled melting of the needle-like crystals, wherein we purposely preserved two 'needles' (indicated by the arrows in Fig. 2(b)) upon heating. After quenching, the preexisted 'needles' did not induce the formation of other edge-on crystals; the surrounding melt, on the other hand, transformed into the flat-on lamellae with a thickness of approximately 10 nm.

The PEO-*b*-PMPCS crystal morphologies have been studied after isothermal melt crystallization at different T_c s. At $T_c < 30$ °C, the crystallization of the diblock copolymer was relatively fast, and the resultant dendritic crystals with ~ 10 nm thickness were similar to those observed in the as-cast ultrathin films. At $T_c > 30$ °C, the PEO-*b*-PMPCS crystallization from the isotropic melt became very difficult, corresponding to a high primary nucleation barrier in the ultrathin films. The self-seeding method was therefore applied, wherein the dendritic crystals obtained by solution casting or melt crystallization at room temperature were used as the precursors. We monitored the morphology change of the precursor dendritic crystals during heating under AFM. When the sample was heated to above 44 °C, a few holes appeared within the crystals, and meanwhile the sharp crystal edges became more or less rounded. At 56 °C or above, the crystals were totally melted to be droplets. Therefore, a T_c of 54.5 °C was chosen to melt most crystals but a few seeds. After self-seeding, the samples were quickly cooled down to the selected T_c s for isothermal crystallization.

On both mica and glow-discharged carbon surfaces, the crystal morphology of the PEO-*b*-PMPCS exhibits the same T_c -dependence. Fig. 3 shows the typical morphologies of the monolayer crystals formed on the carbon surface. The crystals formed at $T_c < 44$ °C are dendritic, of which the 'finger' width and the monolayer thickness increase with increasing T_c [18,19], as evidenced by Fig. 3(a) at $T_c = 25$ °C (thickness of 11.0 nm) and Fig. 3(b) at $T_c = 40$ °C (thickness of 16.8 nm). Fig. 3(d) shows the monolayer lamellae with a thickness of

24.5 nm formed at T_c of 50 °C. The square-shaped morphology is similar to the PEO-*b*-PMPCS single crystals observed in the bulk state in the same T_c region [30]. At 44 °C $\leq T_c \leq 48$ °C, the monolayer lamellae exhibit an intermediate morphology between the square-shaped single crystals and the dendritic ones. Using $T_c = 46$ °C as an example, Fig. 3(c) shows that the separated monolayer crystals with a thickness of 18.2 nm and large lateral dimensions are no longer square-shaped. Note that in the bulk crystallization, the $T_c = 46$ °C is associated with the regime I \rightarrow II transition [30]. This crystal morphology changing from the square-shaped to the dendritic crystals at T_c around 46 °C implies that the ultrathin film crystallization of the PEO-*b*-PMPCS shares a similar surface nucleation mechanism with the bulk crystallization.

For solution crystallizations of the homo-PEOs and PEO diblock copolymers, the square single crystals with four prism faces of {120} planes are the typical morphology [35–37]. To examine the PEO folding directions in the ultrathin films, we performed the SAED experiments on the square-shaped crystals on the carbon surface. Fig. 4 is a TEM image of the crystals formed at 50 °C (where the tiny rods are the PE decoration), with an inset of the SAED pattern. The two pairs of diffraction spots are attributed to the {120} planes of the PEO with monoclinic crystal lattice, which are parallel to the two diagonals of the square-shaped crystals. Therefore, different from the PEO crystals grown from solutions, the four edges of the monolayer crystals are bounded by the (100) and (020) planes. Same as suggested in our previous research of bulk crystallization [30], we consider that the formation of the square-shaped crystals of the PEO-*b*-PMPCS is related to the preferential PEO folding along the (100) and (020) planes on the crystal growth fronts. It is known that in the PEO crystal, the distances of adjacent fold sites of (100) and (020) planes are larger than that of (120) planes. Although after crystallization each PEO stem provides the same surface area disregarding different fold directions, during crystallization, when the PMPCS tablets move to the top and bottom fold surfaces at the crystal growth front, PEO folding along (100) and (020) planes can minimize the PMPCS repulsion from each other.

The SAED results also confirm that the monolayer crystals are flat-on, with the PEO chain direction perpendicular to the substrate surfaces. During the lamellar formation, the PMPCS

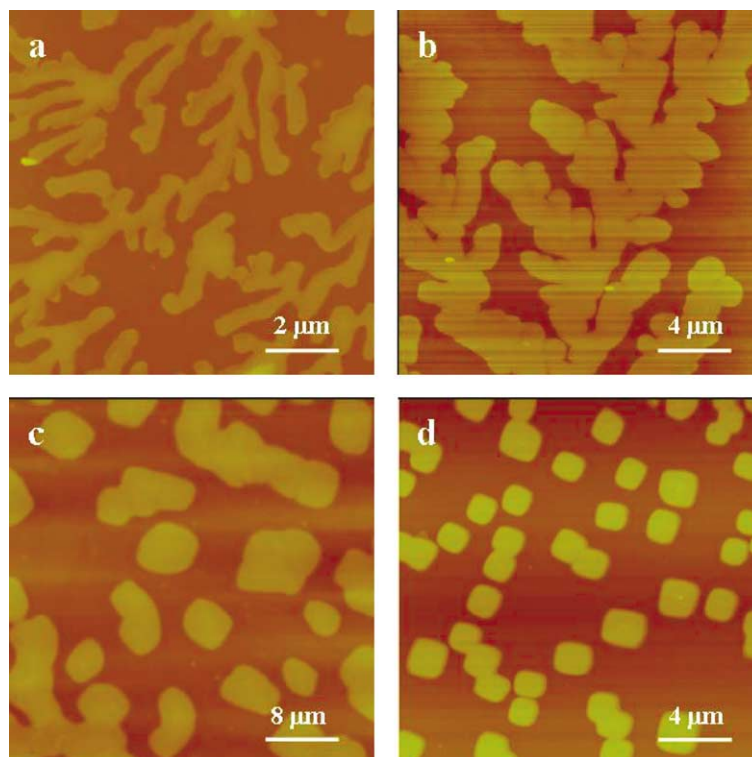


Fig. 3. AFM height images of the PEO-*b*-PMPCS monolayer crystals on glow-discharged carbon surfaces after isothermal crystallization at (a) 25 °C, (b) 40 °C, (c) 46 °C, and (d) 50 °C.

blocks should be randomly distributed on both top and bottom fold surfaces. As a result, the flat-on monolayer crystals have a ‘sandwich’ structure, of which the two amorphous layers are contacted with the substrate and the atmosphere, respectively. Fig. 5(a) presents an AFM phase image of a PEO-*b*-PMPCS single crystal after the PE decoration, wherein a number of LMW PE crystal rods are on the top surface. In the homo-PEO single crystals obtained from solution crystallization, the PE rods decorated thereon are oriented perpendicular to the individual {120} growth faces, evidencing the four microsectors [36]. The random orientation of the PE rods in Fig. 5(a) indicates a featureless top surface of the sample [37]. We further measured the top surface roughness of the monolayer crystals by AFM. In contrast to the IF crystals of the LMW homo-PEO with a mean square average of height deviations (R_q) of ~ 0.15 nm for the top surface, the diblock copolymer studied possesses a much higher R_q of ~ 1.1 nm. Fig. 5(b) shows an AFM height image obtained on a top surface of a monolayer crystal grown at 50 °C. As pointed out by the two red arrows, the height difference between the ‘valley’ and ‘hill’ is approximately 1 nm. In the PEO-*b*-PMPCS bulk crystallization [30], we have proposed that when the average PEO fold number decreases with increasing T_c , to match the increase in the tethering density on fold surfaces, the rigid PMPCS tablets with a thickness of ~ 1 nm and a diameter of ~ 1.7 nm will adjust their neighboring positions up or down with respect to the lamellar surface normal. Here for the monolayer crystal, the ‘hills’ in Fig. 5(b) can be the protruded PMPCS tablets. In addition, the rough top surface may also arise from the polydispersity effect. Note the average DP of PMPCS blocks is

only 5 and the polydispersity of the diblock is 1.07. There is a variation in the number of the MPCS repeating units attached to PEO block, which can also affect the local monolayer thickness.

One interesting observation in Figs. 3(d) and 4 is the well-oriented crystal edges despite the fact that the square-shaped crystals are apart from each other. This phenomenon also existed in the monolayer crystals formed on the mica surface. One may suspect that such oriented growth of single crystals comes from the surface epitaxial effect. However, since the carbon films obtained via evaporation are amorphous in nature,

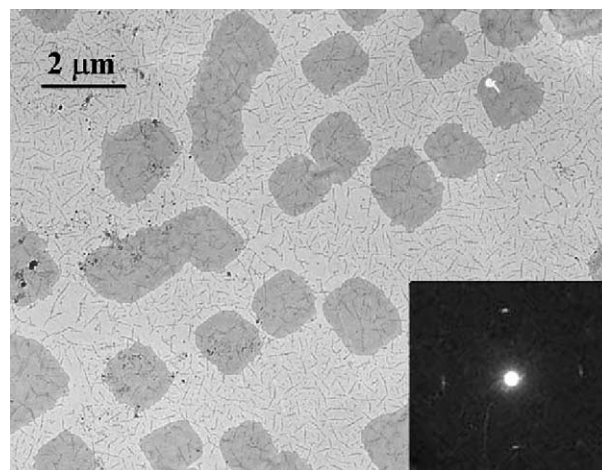


Fig. 4. TEM image of square-shaped crystals on the carbon surfaces after crystallization at 50 °C. The inset is the SAED of the crystals in the correct orientation. The tiny rods are PE decorations.

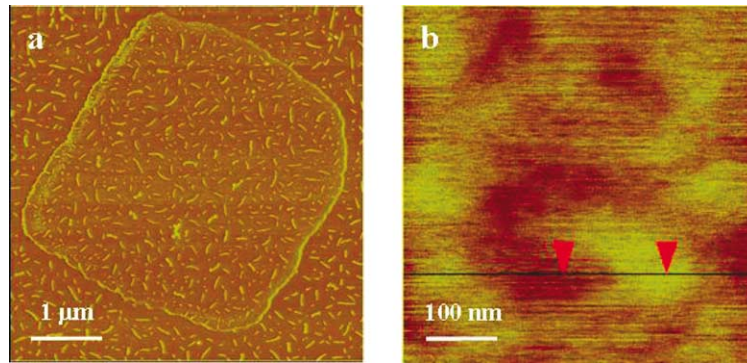


Fig. 5. (a) AFM phase images of a PE-decorated crystal; (b) AFM height image of an area of top crystal surface of a crystal without PE-decoration. The height difference between the two red arrows in (b) is ~ 1 nm. For both (a) and (b), $T_c = 50$ °C.

this epitaxial effect can be precluded. The self-seeding process is likely the reason. In our experiments, the seeds were all from a same monolayer dendritic crystal with large lateral dimensions. When annealed at T_s , the survived tiny seeds stuck to the surfaces had the same a and b directions as the original dendritic crystal did. As a result, they induced the single crystal growth with the same crystalline orientation.

Fig. 6 describes the relationship between the T_c and the monolayer thickness measured by AFM. For both substrates, the monolayer thickness increases monotonously with T_c ; when T_c exceeds 45 °C, the increase in thickness accelerates. Same as found in bulk crystallization of the same diblock copolymer [30], the T_c -dependence of the monolayer thickness reveals that the PEO blocks are essentially non-integrally folded in the crystals. Moreover, it indicates that the confinement along the substrate normal is not strict. During melt crystallization, the monolayer top surfaces may move vertically to accompany the PEO fold length varying with T_c .

Upon the AFM heating experiments, we have investigated the melting behavior of the monolayer crystals. The monolayer dendritic crystals that were imperfect could undergo reorganization or melt/recrystallization during slow heating, and their

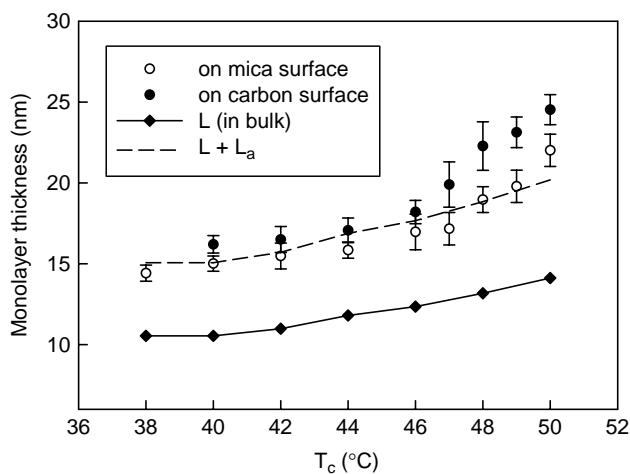


Fig. 6. Relationship between T_c and the thickness of the monolayer crystals on mica and carbon surfaces. For comparison, the long period (L , filled diamond) and the sum of the L and amorphous layer thickness (L_a) of the bulk lamellae (dashed line) are also plotted.

T_m is hard to be unambiguously determined. The crystals formed at $T_c > 44$ °C kept the thickness constant when the temperature approached T_m . Therefore, upon heating, shrinkage of the crystal area indicates the crystal melting. As shown in Fig. 7, the crystal area ratio, A/A_0 (where the A_0 and A are the areas measured at T_c and a temperature during heating), starts to decrease at 54.6 and 54.0 °C for the crystals formed at T_c of 46 °C on the mica and carbon surface, respectively. We take the extrapolated beginnings of A/A_0 decreasing (Fig. 7) as the T_m of the monolayer crystals. Fig. 8 depicts that the T_m of the monolayer single crystals increases with T_c , which is similar to the behavior of the monolayer thickness. At the same T_c , the monolayer crystals on the mica are always 1–2 nm thinner than those on the carbon surfaces, but slightly higher in T_m . This might be related to the more hydrophilic surface of mica.

Occasionally, the formation of multilayer crystals via screw dislocation could also be observed on the mica and carbon surfaces when some big melt droplets were encountered. Fig. 9 shows a set of successive AFM phase images of crystallization at 50 °C on the carbon surface. In Fig. 9(a), a basal lamella is observed, of which the top surface is still covered by melt. As the crystallization progresses, a screw dislocation is initiated at a corner (pointed by the arrow in Fig. 9(b)) of the basal lamella, which will continuously induce the spiral growth (Fig. 9(c)),

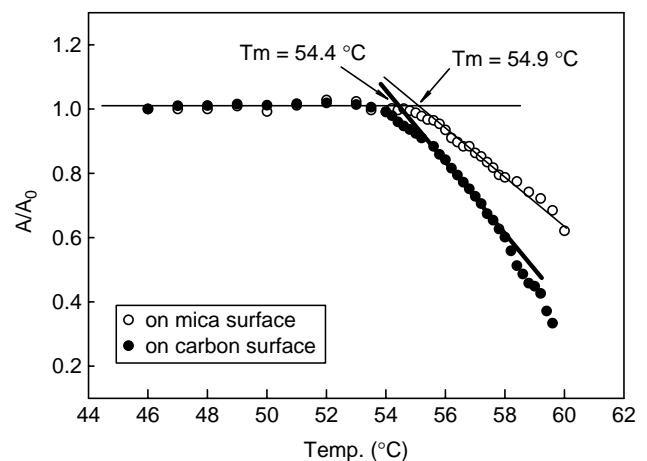


Fig. 7. Changes of the crystal area ratio (A/A_0) during heating for the monolayer crystals originally formed at 46 °C on the mica and carbon surfaces. A_0 and A are the areas measured at T_c and a temperature during heating.

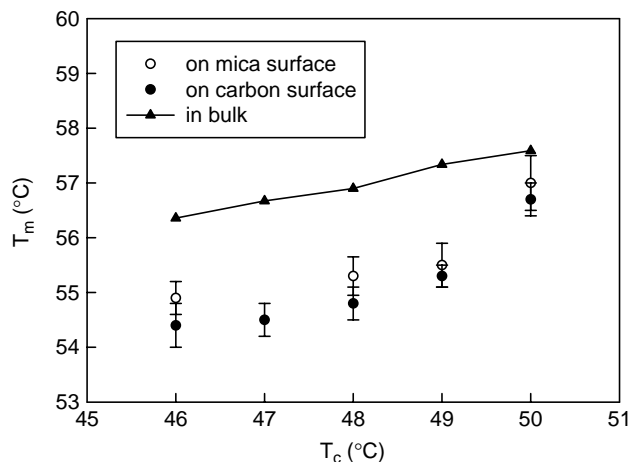


Fig. 8. Relationship between T_c and the T_m of the monolayer crystals formed on the mica and carbon surfaces. For comparison, the filled triangles represent the T_m s of the bulk lamellae.

deplete the melt and form the lamellar terraces (Fig. 9(d)). The height of each terrace is measured to be nearly 24 nm, very close to the thickness of the monolayer crystals formed at the same T_c . We also examined the melting process of the stacked lamellar crystals upon heating (Fig. 10). Fig. 10(a) presents the AFM morphology of lamellar terraces after isothermal crystallization at 50 °C. In the AFM phase image, all the lamellar edges simultaneously turned to be brighter than the inner parts of lamellae when the sample was slowly heated to 56.0 °C, corresponding to a start of the crystal melting (Fig. 10(b) at 56.0 °C as an example). Further heating caused a continuous

shrinkage of the lamellae (Fig. 10(c)), and a complete melt occurred at 60.0 °C (Fig. 10(d)). The above observations suggest that both the multilayer and monolayer crystals share the same T_c -dependence of lamellar thickness and moreover, their T_m is mainly thickness determined. For the stacked lamellae, the upper lamellae possess the interfaces different from those of the bottom one or the monolayer that is directly contacted with the substrates. Thus, their T_m is expected to be slightly different. Due to the limitation of the AFM heating scanning, we were unable to catch such a subtle difference in T_m at this moment.

To compare between the ultrathin film and bulk crystallization, the long period (L) and the amorphous layer thickness (L_a), and the T_m of the same PEO-*b*-PMPCS crystallized from bulk are also presented in Figs. 6 and 8, respectively. For the bulk sample, the L was measured by small angle X-ray scattering, the L_a is calculated based on the L and the volume fraction of the crystalline PEO, and the T_m was deduced by extrapolating the peak temperatures of melting endotherms at different heating rates to 0 °C/min [30]. Interestingly, the monolayer thicknesses on the mica and carbon surfaces are significantly larger than the L of the bulk crystals and moreover, such a difference increases with T_c . For example, at $T_c=46$ °C, the L is 12.4 nm, whereas the monolayer thicknesses on the mica and carbon surfaces are 17.0 and 18.2 nm, respectively. This difference may come from the ‘sandwich’ structure of the monolayer containing two amorphous parts, whereas the L of the bulk crystals only includes one. As a rough approximation, we assume that amorphous layer and the fold length of the monolayer are the

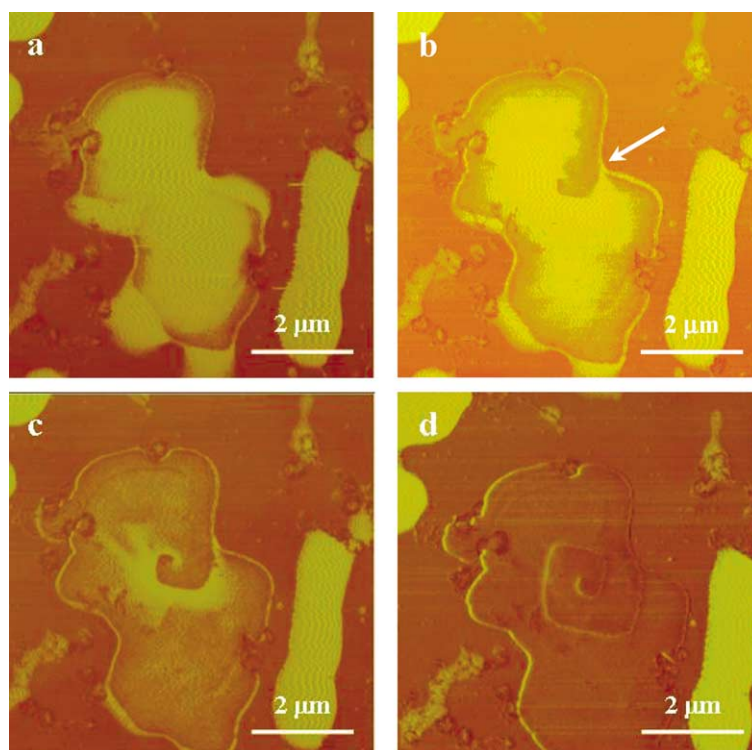


Fig. 9. A set of AFM phase images of the growth of a spiral terraces at 50 °C on carbon surface. The images were recorded at different crystallization time (t_c) of (a) 5 min, (b) 13 min, (c) 35 min, and (d) 80 min.

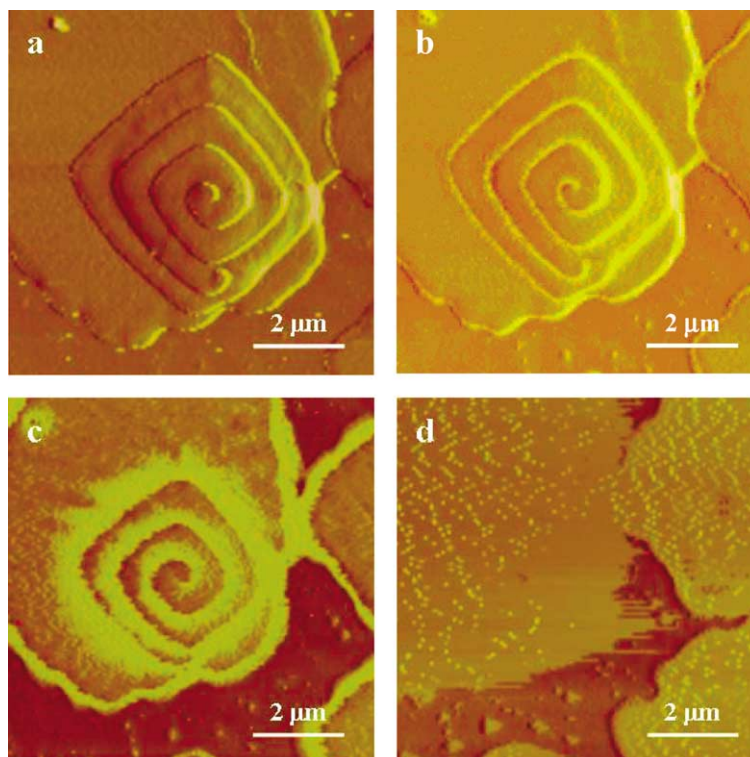


Fig. 10. A set of AFM phase images of a spiral terraces originally formed at 50 °C on carbon surface. The images were recorded at (a) 50 °C, (b) 56 °C, (c) 58 °C, and (d) 60 °C during heating.

same as that of the bulk crystals at the same T_c . Therefore, the overall monolayer thickness can be viewed as the sum of the L and L_a . As indicated by the dashed line in Fig. 6, the calculated monolayer thicknesses (i.e. $L + L_a$) fairly agree with the AFM measurements for the samples on mica at $T_c < 49$ °C and on carbon at $T_c < 46$ °C. However, such an assumption refers to an extreme case, and the calculated data in Fig. 6 only provide a clue to address the effect of the ‘sandwich’ structure on the overall monolayer thickness. In bulk, the inter-lamellar amorphous region is constructed by the PMPCS tablets, PEO folds, and cilia from the two adjacent lamellae. For a monolayer crystal with two amorphous layers, the above assumption that the amorphous thickness is identical to the L_a of the bulk lamellae will lead the amorphous density only half of the bulk one. This density then must be the lowest limit. We consider that without the confinement imposed from the adjacent lamellae, the amorphous parts of monolayer crystals can be loose in packing to a great extent (probably, this is also a reason for the rough surface observed in Fig. 5(b)). On the other hand, the monolayer crystals may also increase the PEO fold length for they lack the confinement on the top surface. In Fig. 6, the deviation between the calculated and measured thickness becomes obvious at the sufficiently high T_c s, which may mainly come from the increase in the PEO fold length.

Nevertheless, the monolayer crystals have a lower T_m than the bulk lamellae at the same T_c (Fig. 8). No full explanation is available at the moment. From a thermodynamic point of view, both the crystalline state and the melt of a monolayer system are different from the bulk. Therefore, many issues may cause a lower T_m of the monolayer crystals by AFM compared with

the T_m of the bulk by differential scanning calorimetry (DSC). The two interfaces of the monolayer crystals, i.e. with the solid substrate and atmosphere, can make the fold surface property differs from that in bulk. For the PEO-*b*-PMPCS studied, the lower T_m of the monolayer crystals might partially result from higher fold surface free energies.

4. Conclusion

In summary, upon using hot stage AFM, the crystal morphology and melting behavior of a LMW diblock copolymer PEO-*b*-PMPCS in ultrathin films have been studied. The ultrathin films on the mica and glow-discharged carbon surfaces were obtained by static dilute solution casting at room temperature. The SAED experiments demonstrate that like homo-PEO, the PEO blocks in the ultrathin films crystallize in the monoclinic crystalline structure. The as-cast ultrathin films are monolayer dendrites with a thickness of 11 nm. In contrast to the glow-discharged carbon surface, the mica surface can also generate needle-like crystals with the feature of edge-on lamellae after solution casting. The melt crystallization from ultrathin films always leads to flat-on lamellae with the PEO chain direction perpendicular to the substrates. At $T_c < 44$ °C, isothermal crystallization of the ultrathin films results into dendritic crystals, of which the ‘finger’ width decreases with decreasing T_c . At $T_c > 48$ °C, square-shaped crystals form, with the (100) and (020) planes as the crystal edges. At 44 °C $\leq T_c \leq 48$ °C, an intermediate monolayer morphology is observed. The monolayer thickness increases continuously with increasing T_c , indicating that the PEO blocks are

non-integrally folded. Compared with the long period of the bulk crystals at the same T_c , the monolayer lamellae exhibit a much larger overall thickness. Most likely, the ‘sandwich’ structure of the monolayer, of which two amorphous layers contact with the substrate and atmosphere, is the reason. Compared with the bulk lamellae, the amorphous layers are rather loose in packing. On the other hand, the monolayer crystals are lower in T_m than the bulk lamellae. The spiral terraces induced by screw dislocation are also observed. Each layer of the terraces possesses the same thickness as the monolayer at the same T_c ; the terraces melt simultaneously, indicating that the melting is mainly terrace thickness determined.

Acknowledgements

This work was supported by the National Natural Science Foundation of China (Grant no. 20025414, no. 20134010, no. 20234020, and no. 20374003). The authors are grateful to Prof. S.Z.D. Cheng for his useful discussions.

References

- [1] Ryan AJ, Hamley IW, Bras W, Bates FS. *Macromolecules* 1995;28:3860.
- [2] Mai SM, Fairclough PA, Viras K, Gorry PA, Hamley IW, Ryan AJ, et al. *Macromolecules* 1997;30:8392.
- [3] Loo YL, Register RA, Ryan AJ. *Phys Rev Lett* 2000;84:4120.
- [4] Zhu L, Chen Y, Zhang A, Calhoun BH, Chun M, Quirk RP, et al. *Phys Rev B* 1999;60:10022.
- [5] Zhu L, Cheng SZD, Calhoun BH, Ge Q, Quirk RP, Thomas EL, et al. *J Am Chem Soc* 2000;122:5957.
- [6] Zhu L, Cheng SZD, Huang P, Ge Q, Quirk RP, Thomas EL, et al. *Adv Mater* 2002;14:31.
- [7] Rottele A, Thurn-Albrecht T, Sommer JU, Reiter G. *Macromolecules* 2003;36:1257.
- [8] Chen HL, Hsiao SC, Lin TL, Yamauchi K, Hasegawa H, Hashimoto T. *Macromolecules* 2001;34:671.
- [9] Hunag YY, Chen HL, Li HC, Lin TL, Lin JS. *Macromolecules* 2003;36:282.
- [10] Opitz R, Lambreva DM, de Jeu WH. *Macromolecules* 2002;35:6930.
- [11] Gao WP, Bai Y, Chen EQ, Zhou QF. *Chin J Polym Sci* 2005;23:275.
- [12] Hong S, MacKnight WJ, Russell TP, Gido SP. *Macromolecules* 2001;34:2876.
- [13] Hong S, MacKnight WJ, Russell TP, Gido SP. *Macromolecules* 2001;34:2398.
- [14] Frank CW, Rao V, Despotopoulou MM, Pease RFW, Hinsberg WD, Miller RD, et al. *Science* 1996;273:912.
- [15] Schonherr H, Frank CW. *Macromolecules* 2003;36:1188.
- [16] Schonherr H, Frank CW. *Macromolecules* 2003;36:1199.
- [17] Sawamura S, Miyaji H, Izumi K, Sutton SJ, Miyamoto Y. *J Phys Soc Jpn* 1998;67:3338.
- [18] Reiter G, Sommer JU. *Phys Rev Lett* 1998;80:3771.
- [19] Reiter G, Sommer JU. *J Chem Phys* 2000;112:4376.
- [20] Reiter G, Castelein G, Sommer JU. *Phys Rev Lett* 2001;86:5916.
- [21] Reiter G, Castelein G, Hoerner P, Riess G, Blumen A, Sommer JU. *Phys Rev Lett* 1999;83:3844.
- [22] Reiter G. *J Polym Sci, Polym Phys Ed* 2003;41:1869.
- [23] Sommer JU, Reiter G. *Phase Transitions* 2004;77:703.
- [24] Massa MV, Dalnoki-Veress K, Forrest JA. *Eur Phys J E* 2003;11:191.
- [25] Dalnoki-Veress K, Forrest JA, Massa MV, Pratt A, Williams A. *J Polym Sci, Polym Phys Ed* 2001;39:2615.
- [26] Zhai XM, Wang W, Ma ZP, Wen XJ, Yuan F, Tang XF, et al. *Macromolecules* 2005;38:1717.
- [27] Buckley CP, Kovacs AJ. In: Hall IH, editor. *Structure of crystalline polymers*. New York: Elsevier; 1984. p. 261–307.
- [28] Cheng SZD, Lotz B. *Philos Trans R Soc London A* 2003;361:517.
- [29] Ye C, Zhang HL, Huang Y, Chen EQ, Lu Y, Shen D, et al. *Macromolecules* 2004;37:7188.
- [30] Huang Y, Wang J, Liu XB, Zhang HL, Chen XF, Zhuang WC, et al. *Polymer* 2005;46:10148.
- [31] Kovacs AJ, Gonthier A. *Kolloid ZZ. Polymere* 1972;250:530.
- [32] Wittmann JC, Lotz B. *Makromol Chem Rapid Commun* 1982;3:733.
- [33] Wittmann JC, Lotz B. *J Polym Sci, Polym Phys Ed* 1985;23:205.
- [34] Takahashi Y, Tadokoro H. *Macromolecules* 1973;6:672.
- [35] Lotz B, Kovacs AJ, Bassett GA, Keller A. *Kolloid ZZ. Polymere* 1966;209:115.
- [36] Chen J, Cheng SZD, Wu SS, Lotz B, Wittmann JC. *J Polym Sci, Polym Phys Ed* 1995;33:1851.
- [37] Chen WY, Li CY, Zheng JX, Huang P, Zhu L, Ge Q, et al. *Macromolecules* 2004;37:5292.